A High Gain Switched-inductor-capacitor DC-DC Boost Converter for Photovoltaic-based Micro-grid Applications

Davut Ertekin

***Abstract*—Maximum power point tracking (MPPT) systems are being developed to produce switching pulses with proper duty ratios for power switches to exert photovoltaic (PV) panels under maximum instantaneous generated power, usually through a traditional DC-DC boost converter. The fundamental issue, particularly for micro-grid and small-scale green DC or AC energy applications, is that the voltage supplied by the MPPT boost converter is insufficient. In order to increase resulting MPP voltage, this research proposes a new high-voltage gain DC-DC boost converter for a cascade connection with an MPPT boost converter. Input side of the proposed converter employs a switched-inductor cell to reduce input current source ripples which is a critical problem in PV systems for high-reliability applications. Additionally, a switched-capacitor cell is used at the converter's output side to boost voltage gain and reduce voltage stress across converter's power switches, which is a crucial factor for longer life of PV panel and proposed converter components, particularly semiconductor devices. Performance of the converter is assessed while taking into account variations in irradiation and temperature brought on by changing weather conditions. A prototype converter at a laboratory scale is utilized and examined. Outcomes of hardware tests support the findings of theoretical and simulation studies.**

***Index Terms*—Boost converter, grid and micro-grid applications, maximum power point tracking, solar energy.**

I. INTRODUCTION

THE important part of energy needs, today is obtained from fossil and nuclear fuels. Protecting the environment, preventing threats that may occur in the future to human life and environmental balance make it necessary to develop and use alternative energy sources [1]–[3]. The sun is the most significant energy source in the world. As a result, solar energy is the most widely used alternative energy source for producing electricity [4]–[10].

When it comes to supplying energy, PV panels are dependent on a variety of factors. In this situation, the system's efficiency will decline due to ideal level of operation of these parameters and a lack of system monitoring. For this reason, numerous studies are conducted in literature to maximize PV system's energy. [11]–[17].

Grid-connected PV systems normally are equipped with a pulse width modulation-based switching DC-DC converter and PV arrays. In these systems, a fast sampling algorithm is designed to calculate instantaneous power measuring instantaneously generated voltage and current of the PV array. MPPT algorithm is chosen based on system complexity, cost, accuracy requirements, and environmental circumstances. Ongoing research strives to improve efficiency and adaptability in extraction of energy from PV systems.

Different algorithms have been investigated which perturb and observe (P&O) [18]–[20], incremental conductance (INC) [21]–[23], fractional open circuit voltage (FOCV) [24], artificial intelligence (AI)-Based algorithms [25], [26], fuzzy logic control (FLC) [27]–[29], and hybrid algorithms [30] are among them.

PV systems are equipped with DC-DC boost converters to enhance generated voltage by the panels. But these MPP converters could not be controlled and enhance voltage of the panel for grid or micro-grid applications. Therefore, a high-voltage gain and efficient boost converter should be cascaded to MPP converter.

Using multiple boost converters in a cascade configuration can effectively increase maximum system voltage gain [31], but it comes at the cost of increased system expenses. This approach also presents the drawback of imposing high voltage stresses on components closer to the load, particularly power components. Furthermore, closed-loop control of these converters, known as Constant Power Loads (CPL), is more complex compared to standard DC-DC converters.

Switched capacitor cells have been recommended as a means to enhance DC voltage gain in converters [32], [33]. By employing specific switching techniques, output voltage and input current ripples can be kept within an acceptable range. However, implementing such switched-capacitor-based DC-DC converters necessitates a significant number of controlled switches, which may increase complexity and cost of the system.

To address weight and cost concerns, applying small inductors in the DC-DC converter structure can be beneficial [34], [35]. By replacing existing converter coils with switched inductors, voltage of DC-DC converters can be increased. Coupled inductors in non-insulated converters can further boost voltage gain. Nonetheless, these circuits require incorporation

Manuscript received November 29, 2022; revised May 26, 2023; accepted August 3, 2023. Date of online publication December 26, 2023; date of current version November 20, 2024.

D. Ertekin (corresponding author, email: davut.ertekin@btu.edu.tr) is with the Power Electronics Center of Electrical and Electronics Engineering Laboratories, Bursa Technical University, Bursa, Turkey.

DOI: 10.17775/CSEEJPES.2022.08440

of snubber circuits to absorb energy stored in the inductor, adding complexity but improving efficiency.

Use of an active clamp technique in these converters, combined with voltage regulation through power switches, enhances system efficiency by discharging leakage energy stored in the inductor at the load [36]. However, converter's input current becomes completely pulsed, potentially exacerbating leakage inductance and parasitic capacitance. Additionally, as inductor conversion ratio increases, number of leakage inductors in converter coils also rises, resulting in increased voltage across power switches and reduced efficiency.

In recent years, use of inductor-capacitor switching converters has gained significant attention. This approach involves charging energy storage elements simultaneously, when power switches are in on-state, followed by discharging all the energy to the load in the next time interval, thereby significantly increasing converter voltage gain. Some studies propose integrating switched-inductor blocks into standard DC-DC converter structures to achieve higher voltage gain [37]–[40]. These circuits offer almost continuous input current and relatively simpler converter models, facilitating closed-loop control. However, when the power switch is in off-state, the entire output voltage is applied across the switch, limiting use of low-voltage transistors to reduce converter losses.

Several transformer-less DC-DC converters with high voltage gain have been suggested to reduce power switch voltage stress [41]. These circuits charge two similar inductors in parallel and series during on and off states of the power switch, respectively. While these converters achieve a maximum voltage gain approximately equal to half of output voltage, the possibility of modular implementation to further increase gain and reduce switch voltage stress has not been thoroughly explored. Furthermore, when the converter diode is in off-state, total output voltage drops across it, making it impossible to use fast Schottky diodes to minimize switching losses.

In this study, to leverage both switched capacitors and inductors, a high-gain transformer-less DC-DC converter has been proposed. This approach aims to increase converter gain while reducing power switch voltage stress. Additionally, due to the power switch being in series with input source through the inductors, input current has less stress with a continuous form that decreases input current ripples and enhances the life cycle of the panel and semiconductor components of the circuit. Also, an improved P&O MPPT algorithm is presented for the primary MPP converter.

This study consists of these parts: the proposed MPPT design and suggested boost circuit are analyzed in Section II, and Sections III and IV present findings and conclusions, respectively.

II. Proposed MPPT Algorithm and DC-DC Converter

A. MPPT Method

The Perturb & Observe algorithm is a well-known MPPT technique for photovoltaic (PV) systems. It operates by perturbing the operating point of the PV system and observing resulting change in power output. Algorithm continuously adjusts operating point by either increasing or decreasing PV system's voltage or current and selects direction that leads to higher power output.

One advantage of Perturb & Observe algorithm is its simplicity, as it does not require detailed knowledge of PV system's characteristics. However, algorithm may suffer from oscillations around maximum power point, especially under rapidly changing environmental conditions.

It is important to choose an appropriate perturbation step size to strike a balance between tracking speed and stability. A DSP-based microcontroller is used for the proposed converter with 80 MHz sapling rate. This feature gives the opportunity of fast comparing and adjusting correct perturbation step size. The proposed algorithm changes value of the duty ratio for power switches according to difference between measured and stored values of duty cycles. Since frequency of the sampling is high enough, more accurate duty ratio is selected.

Block diagram of the proposed simple P&O algorithm and used DSP controller is shown in Fig. 1. This algorithm compares current power value ($P(t)$) with power value obtained in previous sample ($P(t-1)$). If current power value is greater than previous power value ($P(t) > P(t-1)$), it indicates PV system is moving closer to MPP. In this case, the algorithm continues to perturb operating point in the same direction (increase or decrease voltage or current) to track MPP.

If current power value is lower than previous power value ($P(t) < P(t-1)$), it suggests PV system has moved away from MPP. In response, algorithm changes direction of perturbation, it reverses change in voltage or current to bring system back towards the MPP.

Algorithm repeats this process at each sampling interval, continuously adjusting operating point based on power comparison to maximize power output.

B. Proposed Converter

The recommended converter is shown in Fig. 2. This figure shows connection of the proposed converter with integration of PV panel and MPPT boost converter. This figure simply shows after tracking power at MPP by conventional MPP boost converter, the proposed converter acts to enhance generated DC voltage and fix it. This circuit topology includes two power switches M_1 and M_2, three inductors L_1, L_2, and L_3, five capacitors C_1 to C_4, and Co, and six power diodes D_1 to D_6. The main power switch is illustrated with M_2 index, and M_1 is an auxiliary switching component. For this converter, both power switches will be activated and deactivated at the same time intervals.

The main role of the auxiliary switch is reducing voltage stress that will impose on main switch. Analysis for continuous conduction mode (CCM) of the proposed converter is considered for load side. This converter includes two on and off-operating states in CCM. Operating modes are described below.

C. ON and OFF-states and Operating Modes of the Converter

First State: When switches are activated, diodes D_2, D_3, D_4, and D_6 switch to off and D_1 and D_5 to on-state. Anode pins of diodes D_2 and D_3 are connected to earth so they stay

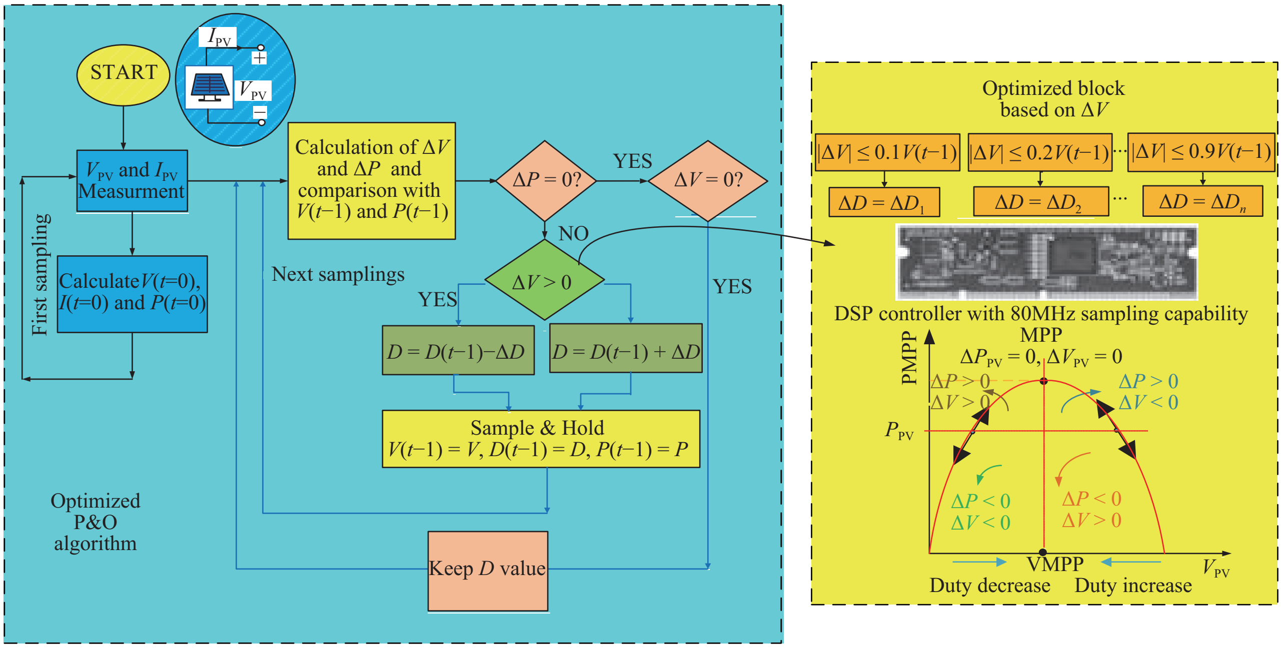

Fig. 1. Modified perturb and observe algorithm flowchart for MPPT approaches in PV systems.

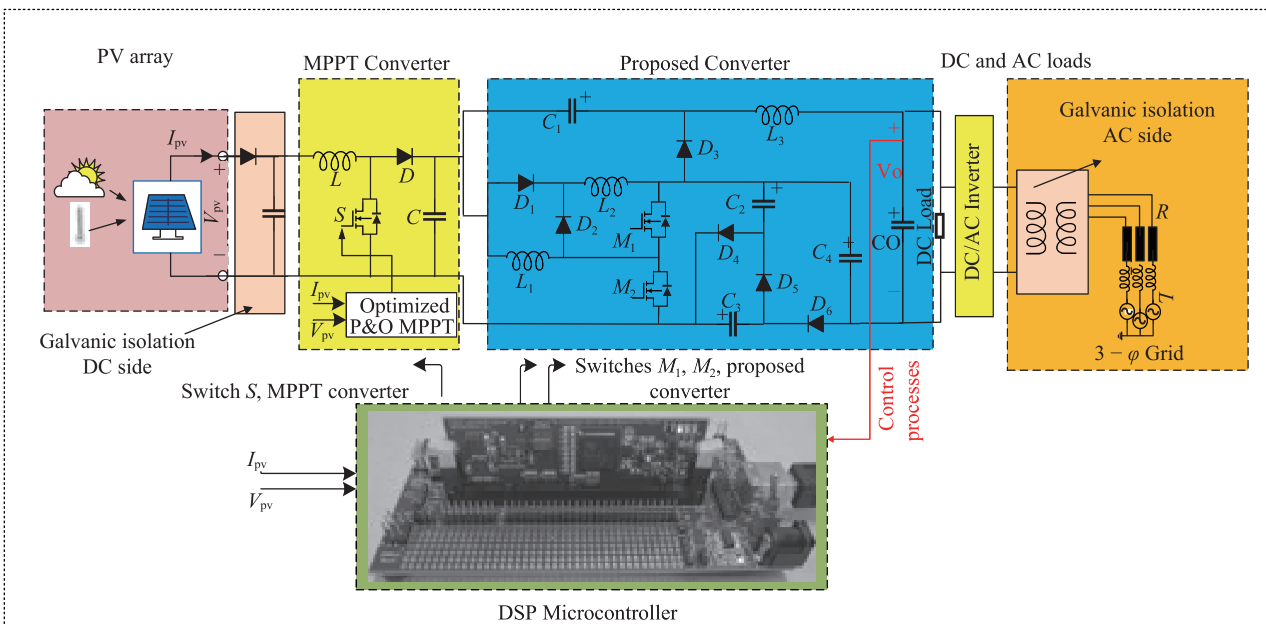

Fig. 2. Proposed switched-inductor-capacitor DC-DC boost converter and integration of this converter with PV array, MPPT converter, and DC and AC loads.

at off-mode. Equivalent circuit for this situation is shown in Fig. 3(a). As observed, input inductors L_1 and L_2 will be parallel and charged linearly by input voltage. In this mode, voltage at C_3 is discharged in capacitor C_2 via diode D_5, and capacitor C_4 is discharged. The reason is positive plates of capacitors C_2 and C_4 are connected to earth. In this mode, inductor L_3 starts to be charged because voltage at L_3 is positive and current of capacitor C_1 is discharging on this inductor. According to KVL laws for this state of operation and polarity of capacitors, the following equations can be obtained.

$$V_{\text{in}} = V_{L1} = V_{L2} \tag{1}$$

$$V_{\text{in}} = V_{L2} + V_{C2} - V_{C3} \tag{2}$$

$$V_{C2} - V_{C3} = 0 \rightarrow V_{C2} = V_{C3} \tag{3}$$

$$-V_{\text{in}} - V_{C1} + V_{L3} + V_O - V_{C4} = 0 \tag{4}$$

$$V_{L3} = V_{\text{in}} + V_{C1} - V_O + V_{C4} \tag{5}$$

Input and output voltages are denoted by V_{in} and V_O in preceding equations. Voltages across the L_1, L_2, and L_3 inductors are represented by V_{L1}, V_{L2}, and V_{L3}, while voltages across the C_1, C_2, C_3, C_4, and Co capacitors are represented by V_{C1}, V_{C2}, V_{C3}, V_{C4}, and V_{CO}.

Second State: For this mode of operation, equivalent circuit

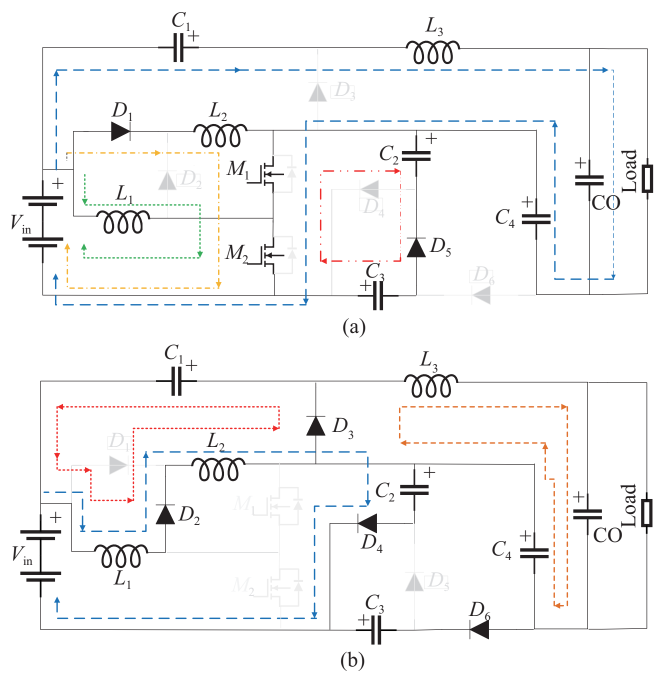

Fig. 3. Configuration of the proposed boost converter and components states when power switches are (a) activated and (b) deactivated.

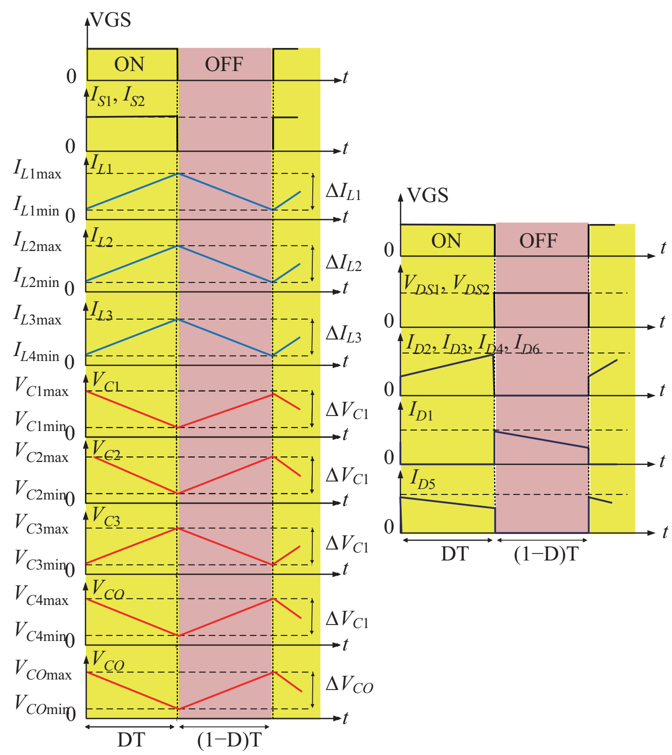

Fig. 4. Component waveforms of the designed transducer in CCM operating mode for proposed converter.

is shown in Fig. 3(b). In this case, the switch is passivated, and power diodes D_1 and D_5 operate in off and other diodes in on-modes. By considering the serial connection for input inductors, voltages across the inductors L_1, L_2 start to discharge, voltages across capacitors C_1, C_2, and C_4 begin to be charged and C_3 discharged. Furthermore, inductor L_3, which was charging for first operating mode, will be discharged for this situation because it endures a negative voltage base on charging states of capacitors C_1 and C_4. Equations of elements for this state can be obtained as follows:

$$V_{\text{in}} = V_{L1} + V_{L2} + V_{C2} \rightarrow V_{L1} = V_{\text{in}} - V_{L2} - V_{C2} \quad (6)$$

$$V_{C4} = V_{C2} + V_{C3} \quad (7)$$

$$V_{C1} = -V_{L1} - V_{L2} \quad (8)$$

$$V_{L3} = V_{C4} - V_O \quad (9)$$

$$V_{L2} = V_{C1} - V_{L1} \quad (10)$$

Figure 4 depicts current and voltage states for components of the proposed circuit based on given equations and simulation results. The above illustration shows all inductors are charged and discharged at the same time. Capacitors C_1, C_2, C_4, and C_O charge and discharge at the same time intervals, whereas capacitor C_3 charges in the opposite direction as other capacitors. Also, when diode D_1 is deactivated, diodes D_2, $D3$, D_4, D_5, and D_6 are active, and vice versa.

D. Voltage Gain for CCM Operation Mode

Duty cycle for a power component is defined as follows:

$$D = \frac{T_{\text{on}}}{T} \quad (11)$$

In this equation, T_{on} is equal to DT, and is known as time interval a power switch is activated. Switching time period is shown by T. According to steady-state voltage equilibrium theorem; value of voltage for an inductor with a time period including on (0 to DT) and off (DT to T) states time intervals are equal to zero. By considering this fact for inductor L_1 and through (1), and (6):

$$\int_0^{DT} (V_{\text{in}})\mathrm{d}t + \int_{DT}^{T} (V_{\text{in}} - V_{L2} - V_{C2})\mathrm{d}t = 0 \quad (12)$$

By considering this fact both L_1 and L_2 are charging at the DT time interval with input voltage and discharging in $(1 - D)T$ time interval by the same values of $L_1 = L_2$, one can obtain $(V_{L1} = V_{L2})$, so by (12), voltage in capacitors C_2 and C_3 can be obtained as follows:

$$V_{\text{in}} DT = \frac{V_{\text{in}} - V_{C2}}{2}(1 - D)T = 0 \rightarrow V_{C2} = V_{C3} = \frac{V_{\text{in}}(1 + D)}{(1 - D)} \quad (13)$$

Based on (7), voltage in capacitor C_4 equals:

$$V_{C4} = \frac{2V_{\text{in}}(1 + D)}{1 - D} \quad (14)$$

By considering Fig. 3, one can write:

$$V_{L1} + V_{L2} + V_{C2} - V_{\text{in}} = 0 \text{ and } V_{L1} + V_{L2} + V_{C1} = 0 \quad (15)$$

Then, by replacing (13), voltage across capacitor C_1 will be obtained as below:

$$V_{C1} = \frac{2V_{\text{in}} D}{(1 - D)} \quad (16)$$

Based on laws described as second voltage balance rule, according to Figs. 3(a) and 3(b) and (5) and (9), one can write for inductor L_3:

$$\int_0^{DT}(V_{\text{in}}+V_{C1}-V_O+V_{C3})\mathrm{d}t + \int_{DT}^{T}(V_{\text{in}}+V_{C1}-V_O+V_{C3})\mathrm{d}t=0 \tag{17}$$

Therefore, by replacing values of parameters V_{C1} and V_{C3} in this equation, DC voltage gain of the proposed converter for CCM operating mode can be presented as follows:

$$M_{\text{CCM}}=\frac{V_o}{V_{\text{in}}}=\frac{2D+2}{1-D}=2\frac{1+D}{1-D} \tag{18}$$

Galvanic isolation is an important concept in PV systems because it ensures electrical safety and protects sensitive components. It entails dividing two or more electrical circuits to prohibit direct current (DC) or alternating current (AC) transition between them while permitting signal or power transmission.

Galvanic isolation is usually used in PV systems between DC side (solar panels and inverters) and AC side (grid or loads). Isolation is required for electrical safety, noise and interference reduction, and grounding compatibility. There are several methods for achieving galvanic isolation in PV systems, including use of transformers, and capacitive and magnetic coupling. At input side of the converter, a combination of a power diode and a capacitor acts as a galvanic isolator to prevent reverse currents or voltage spikes on the PV system. Although voltage conversion form DC to AC and grid connection problems are not the subject of this study, when it comes to grid connection, a transformer can be added between inverter output nodes and grid input nodes.

E. Efficiency Calculations

Internal resistance of circuit components can be used to improve converter's efficiency. When power switch is turned on, this resistance is denoted by r_{DS} for diodes, R_{C1} to R_{C4} and R_{CO} for capacitors, and r_{L1}, r_{L2}, and r_{L3} for inductors. Diode threshold voltages are represented by V_{F1} to V_{F6}. Total losses can be computed for all components as follows:

$$\begin{aligned}P_{\text{loss}}&=P_{\text{switch}}+\sum_{u=1}^{6}(P_{RF})_{D_u}+\sum_{u=1}^{6}(P_{VF})_{D_u}+\sum_{u=1}^{6}P_{RC_u}\\&\quad+P_{rL_1}+P_{rL_2}+P_{rL_3}+P_{RC_o}\end{aligned} \tag{19}$$

Efficiency equation for converter can be obtained in the following ways:

$$\eta=\frac{P_o}{P_o-P_{\text{loss}}}=\frac{1}{1+\frac{P_{\text{loss}}}{P_o}} \tag{20}$$

By calculating switching losses for power semiconductor devices and dynamic losses for all components, efficiency can be found as follows:

$$\eta=\frac{1}{1+\frac{\varphi}{RD(1-D)^2}+r_{C_o}\frac{D^2(1-D)^2R}{12(2+2D)^2L_3^2f_s^2}+\frac{f_sC_SV_{\text{in}}^2}{(1-D)^2RI_o^2}} \tag{21}$$

φ in (21) can be summarized with (22) as follows:

$$\begin{aligned}\varphi&=r_{\text{DS}}(2+2D)^2+(1-D)(R_{F1}+R_{F2}+R_{F4}+R_{F6})\\&\quad+\frac{(1-D)}{I_o}\sum_{u=1}^{6}V_{Fu}+(1-D)^2R_{F3}+(1-D)\\&\quad+(1-D)(r_{C_1}+r_{C_4})+(1-D)(r_{C_2}+r_{C_3})\\&\quad+(2+2D)^2R_{L_1}(2+2D)^2R_{L_2}+(1-D)R_{L_3}\end{aligned} \tag{22}$$

F. Control Method, PI Controller

Proportional Integral (PI) is used as controller for the proposed DC-DC boost circuit in this study. Simplicity of implementation and obtaining a deep mathematical behavior of circuit components are among the most important reasons for PI controller selection.

DSP-based, TMS320F28379D microprocessor is used for the laboratory tests with advantages such as being compatible with Matlab/Simulink software, high integration reliability, cheap cost, high processing speed, and low power consumption.

G. Performance Evaluation of the Proposed Converter

Table I compares the proposed converter to other boost converters [42]–[50] in order to evaluate the proposed converter's features. For safe comparison, all of these converters are in the same classification and incorporate switched-capacitor or switched-inductor cells. According to table results, despite the fact the suggested converters in references [43], [45]–[47], and [49] only contain one power switch, voltage gain of the proposed converter is significantly higher, especially for longer duty cycles. Reference [44] converter includes four power switches that necessitate a more sophisticated controller design. Number of inductors in all of converters in Table I is comparable; however, the proposed and converter in [46] have the most capacitors, and suggested converter in [47] has the most power diodes in its construction. The proposed converter can provide greater DC voltage gain while reducing voltage stress across power switches. Fig. 5 depicts voltage gain diagram for all of converters listed in Table I. As can be observed from the graph, gain of the proposed converter is significant at all duty ratio scales. It depicts voltage gain of converters in Table I graphically for a better understanding of converters' performance. This chart clearly illustrates the suggested converter has a significant gain when compared to converters in the same classification, such as switched-capacitor or switched-inductor cells. For example, at $D=0.6$ and 0.9, the proposed SL-SC-based converter theoretically achieves gain equivalent to 8 and 38 times input voltage source, which is significant and exceeds gain of several converters in this table and figure.

Value of voltage stresses across semiconductor devices, which can affect converter's reliability and longevity, is one of the most essential features of the converter.

Figure 6(a) shows voltage stress across primary power switch is substantially lower than in other converters, especially for high-voltage applications, and that it functions perfectly. This graph demonstrates only roughly 10% of output

TABLE I
COMPARISON FOR PROPOSED AND OTHER BOOST CONVERTERS

Topology	Num. of elements L C D S	Total Num. of power components	Voltage gain	Voltage stress on main switch	Current stress across main switch	Topology of converters	Control method and details
[42]	4 5 3 2	14	$\frac{1+3d}{1-d}$	$\frac{V_o}{1+(n+1)d}$	$\frac{d+\frac{nd}{2}}{1-d}I_o$	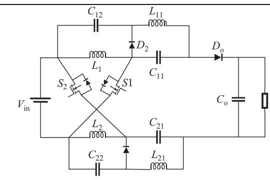	There is no information about the control circuit.
[43]	3 3 5 1	12	$\frac{d(1+3d)}{(1-d)}$	$\frac{(1+d)}{d(1+3d)}V_o$	$\frac{2d(3+d)}{(1-d)}I_o$	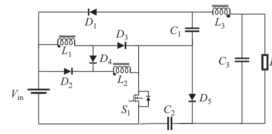	Closed-loop PWM controller, according to circuit mathematics
[44]	3 2 1 4	10	$1+\frac{2d}{1-(d-d_{\text{loss}})}$	–	–	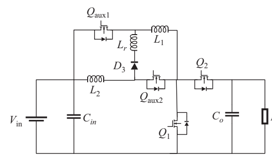	There is no information about the control circuit.
[45]	4 3 2 1	10	$\frac{1+nd}{1-d}$	$\frac{V_O}{(1+n)d}$	$\left(\frac{1+n}{1-d}\right)I_o$	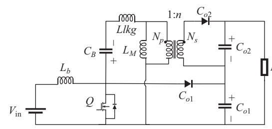	There is no information about the control circuit.
[46]	2 5 4 1	12	$\frac{2+nd}{1-d}$	$\frac{(1-d)V_O}{(2+nd)}$	$\frac{M_{\text{CCM}}-1}{M_{\text{CCM}}}\sqrt{\frac{M_{\text{CCM}}+n}{M_{\text{CCM}}-2}}$	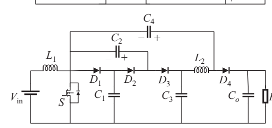	Steady state based PI controller, according to circuit mathematics
[47]	2 4 7 1	14	$\frac{3+d}{1-d}$	$\frac{dV_o}{2}$	$\sqrt{\sqrt{d}\frac{3+d}{1-d}}I_o$	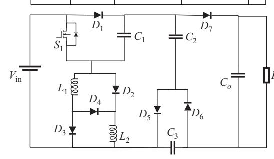	PI controller, according to circuit mathematics
[48]	2 2 3 2	9	$\frac{1+d}{1-d}$	$\frac{d}{1+d}V_o$	–	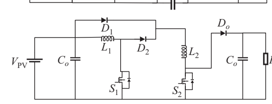	2-model predictive control based MPPT algorithm
[49]	5 4 3 1	13	$\frac{2n-1}{(1-d)(n-1)}$	$\frac{n-1}{2n-1}V_o$	–	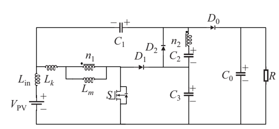	P&O algorithm for MPPT controller, simple sampling and comparing switching signals, No need for circuit equations
[50]	2 4 4 2	12	$\frac{2}{(1-d)^2}$	$\frac{V_o}{4}$	$\frac{I_O}{(1-d)^2}$	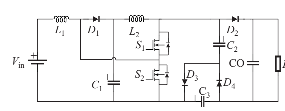	Fuzzy logic controller, No need for circuit equations
Proposed	3 5 6 2	16	$\frac{2(1+D)}{(1-D)}$	$\frac{V_O(1-D)}{2(1+D)}$	$\frac{(2+2D)I_o}{\sqrt{D}(1-D)}$	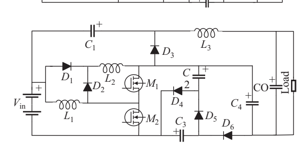	PI controller, according to circuit mathematics

voltage decreases over switch M_2, indicating converter is ready for high-power applications.

The least possible current stress for power components is another feature of a good converter. Minimum level of current ripples, especially for the PV-connected converters on the source side, current of power switches, and also current for diodes all are important. Fig. 6(b) shows current stress for switch M_2 in relation to output current. It also displays the same characteristic as some of converters in Table I. This figure shows that as is expected, theoretically for longer duty ratio and under high-power applications, current of switches are being more and more. State of this stress for switch M_2 in the suggested converter shows current is acceptable and is comparable with other good topologies in the same classification. Because some references in Table I do not have a current equation or values are large or small and cannot be compared with other sources, relevant current or voltage equation is not drawn in the figures.

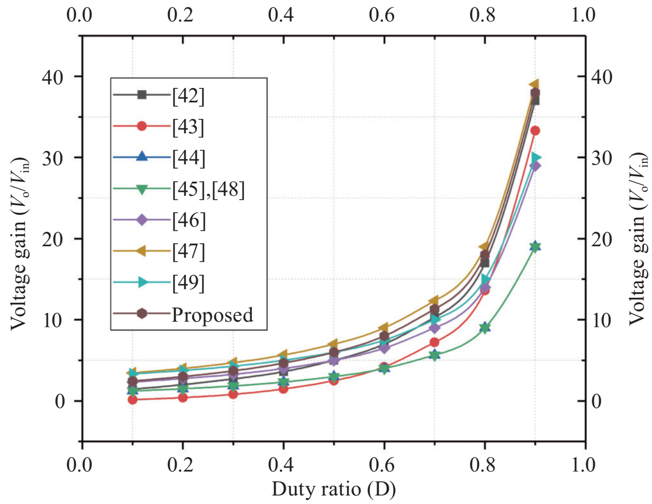

Fig. 5. Voltage gain graphics for the proposed and other converters in Table 2.

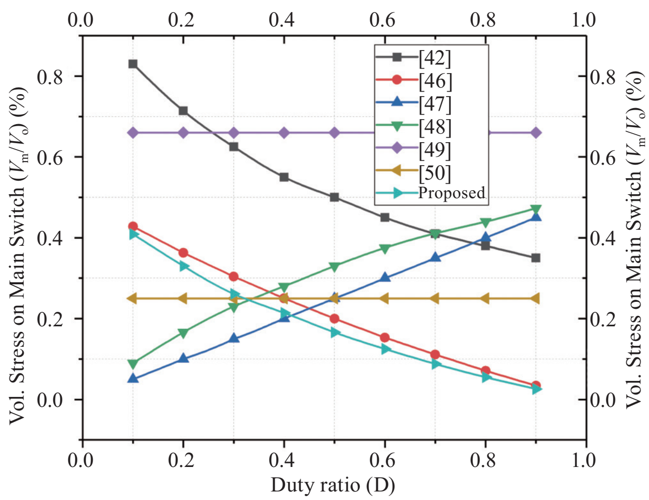

(a)

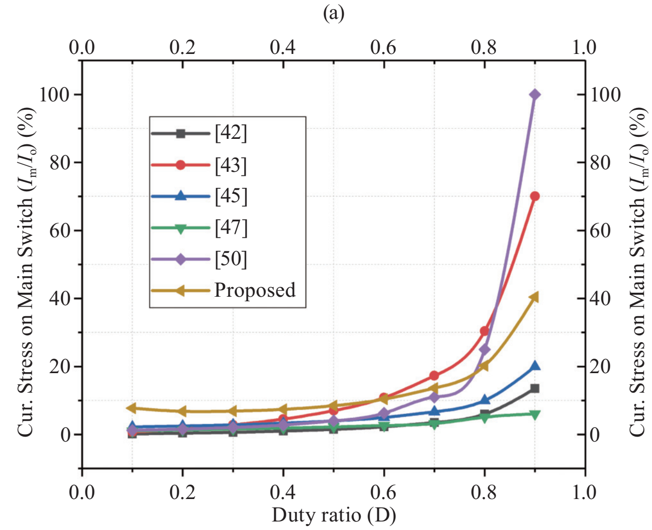

(b)

Fig. 6. (a) Voltage and (b) current stresses for the main switch of the proposed and other converters in Table 2.

In addition, controller process model for circuits described in this table has been supplied. While no controller information is provided for circuits in references [42], [44], [45], PI controller is employed for converters in references [43], [46], [47], and the proposed converter in this study. PI controller was developed after a thorough mathematical analysis of the circuit, as controllers with approximate, K_P and K_i coefficients could not provide an accurate control mechanism. A simple sampling and comparing controllers for circuit in [49] and a fuzzy logic controller for the converter in [50] are provided, both of which do not require converter's equations. [48] describes a 2-model predictive control-based MPPT algorithm that requires accurate forecasting of converter components' currents and voltages.

III. Results and Discussion

This section is investigating performance of the proposed converter under optimized MPPT technique. In first stage, generated voltage by MPPT boost converter under different irradiances and temperatures is evaluated. Fig. 7(a) shows a scenario of received irradiance by a Jiyangyin HR-200W/24V PV panel. This figure shows that start time irradiance equal 750 W/m^2 is received by panel for 1 second. For the next time intervals with a 1-second duration, the irradiance changes to 850 and 1000 W/m^2. Power by the mentioned panel is presented in Fig. 7(b) for these irradiances and also transferred power by the MPPT and proposed converters are reported in this figure. Under W/m^2, generated power by the panel is greater for larger irradiances, and therefore transferred power by the boost converters is enhanced.

Figure 7(c) depicts voltage values generated by the panel and other boost converters. Where voltage of the panel and MPPT converter is about the same, the proposed converter can successfully increase voltage. This figure depicts performance of the proposed converter without taking into account controller and intends to demonstrate how converter can enhance generated DC voltage by the panel and MPPT converter. Fig. 7(d) presents performance of the proposed topology under 35°C temperature. As expected, as the temperature rises, generated power drops, as do power values intended to be transferred to the load. The same irradiation levels are applied to the panel at the same times under the new temperature. Fig. 7(e) shows generated voltage by the panel and converters for variable irradiance and of 35°C the temperature for the Jiyangyin HR-200W/24V PV panel. This figure clearly demonstrates success of the proposed converter in increasing generated small voltages by the panel and MPPT converter and offers a voltage near to generated voltage at 25°C. Fig. 8 depicts predicted topology's performance with more power and the same irradiance and temperatures. Through parallel connection, two Jiyangyin HR-200W/24V PV panels are considered. Generated power will be doubled under this new working state; thus, we may expect higher voltages. Figs. 8(b) and 8(c) represent generated power and voltages of the panels at 25°C. Panels generate 400 W of power at optimal working conditions of 1000 W/m^2 and 25°C of temperature. Under this operational mode, the suggested converter transfers roughly 365 W, resulting in an efficiency of close to 92.5 percent. This graph indicates as input power increases, so does efficiency. Simulation results demonstrate that for 1 kW

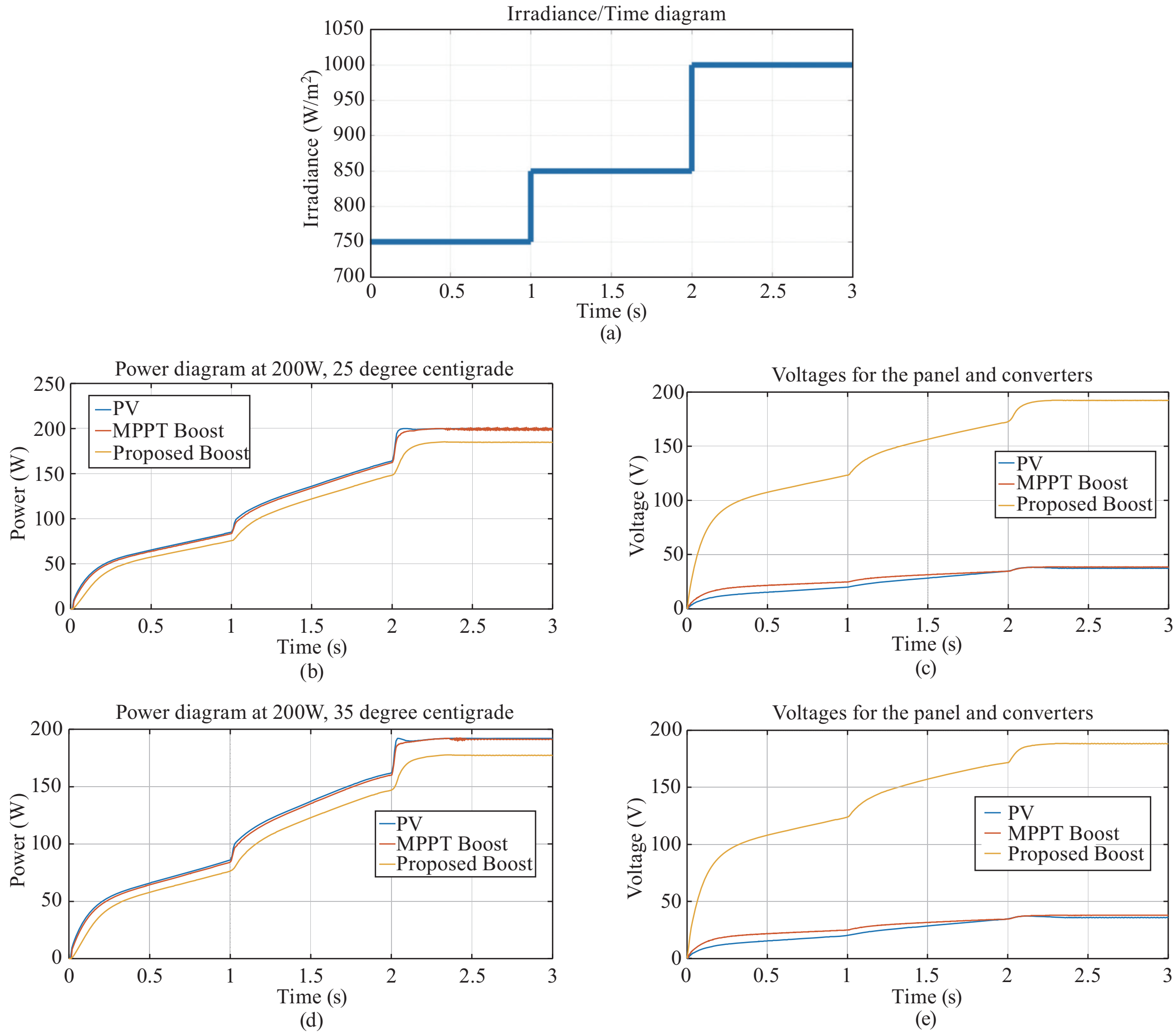

Fig. 7. The (a) irradiance and generated (b) power and (c) voltage under 25°C of the temperature and generated (d) power and (e) voltage under 35°C of the temperature.

of power, 5 parallel panels achieve an efficiency close to 98 percent. Greater DC voltages can be obtained by using greater input voltages, as shown in Fig. 8(b).

The same results can be obtained with 400 W input power and a temperature of 35°C. Figs. 8(c) and 8(d) demonstrate outcomes for this operating situation. Because panel's best performance is realized at temperatures below 25°C, higher temperatures are projected to yield lower powers. Fig. 8(c) demonstrates this. Boosted voltage by the proposed converter is significant when considering voltage of the panel, and more than 6 times the voltage gain is attained under the 0.5 duty ratio for the proposed converter. Higher DC voltages are simply feasible with higher duty cycles. Fig. 9 displays performance of the proposed boost converter using a PI controller to provide a fixed 300 VDC for converter's output voltage. Input voltage is set to 30 volts of direct current. Converter's other specs are the same as in Table I. Fig. 9(a) shows current status of input and output voltages. Fig. 9(b) depicts converter's input and output currents. This figure validates theoretical findings since, with a DC voltage gain of close to ten times, input current should be greater than output voltage under constant power.

Figure 9(c) illustrates voltage stress across primary power switch (S_2). This graph indicates voltage between the switch S_2's drain-source pins approaches half output voltage. Fig. 16(d) also depicts current pressures for both switches.

This diagram illustrates currents of the switches are nearly the same and that average current values are close to each other. Figs. 9(e) and 9(f) show voltage across diodes D_1 to D_6. These findings strongly confirm theoretical expectations and equations presented.

Figure 9 depicted current state of all components. Figs. 9(e) and 9(f) simply demonstrate these results are correct; for example, when diode D_1 is activated, diode D_3 is deactivated, and when diode D_4 is on, diode D_5 is off.

Figure 10 demonstrates controller's performance as voltage of input source changes. This status is taken into account when PV panel generates varying DC voltages. Fig. 10(a) shows how voltage of input source changes from 45 to 35 VDC in 2.5 V steps at $t = 1$, 2, 3, and 4 seconds. The suggested boost converter presents a fixed DC voltage for all ranges of input voltage source and findings reveal no substantial under/ overshoots are recorded at change times for all these ranges

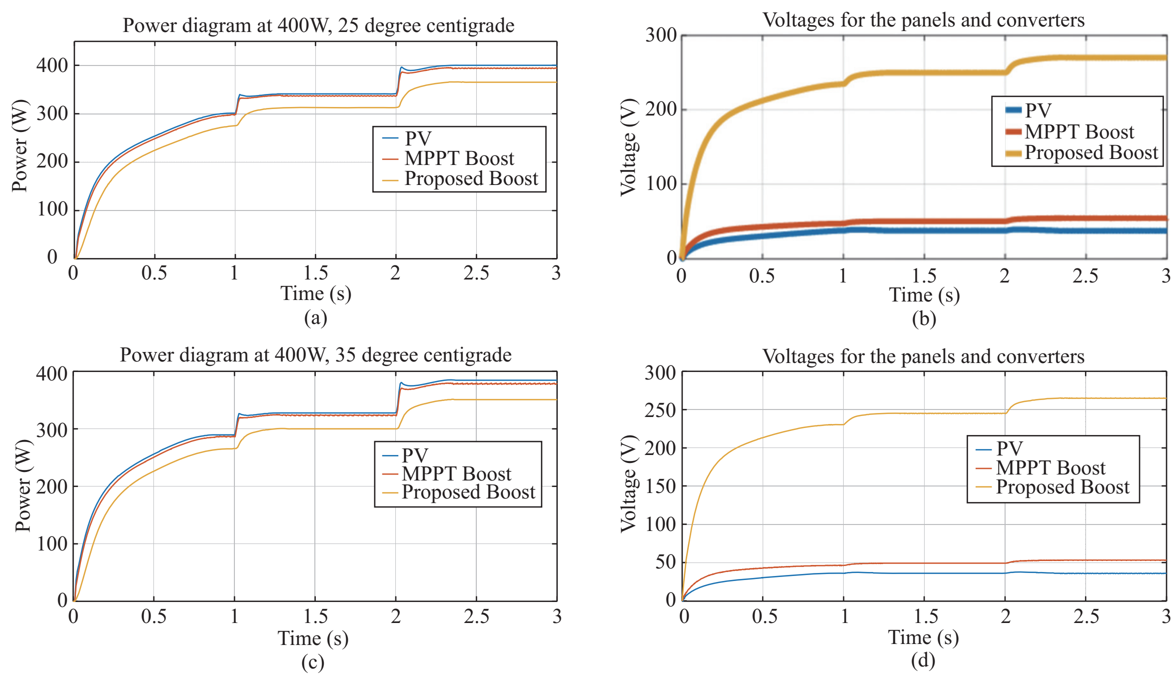

Fig. 8. The generated (a) power and (b) voltage under 25°C of the temperature and generated (c) power and (d) voltage under 35°C of the temperature.

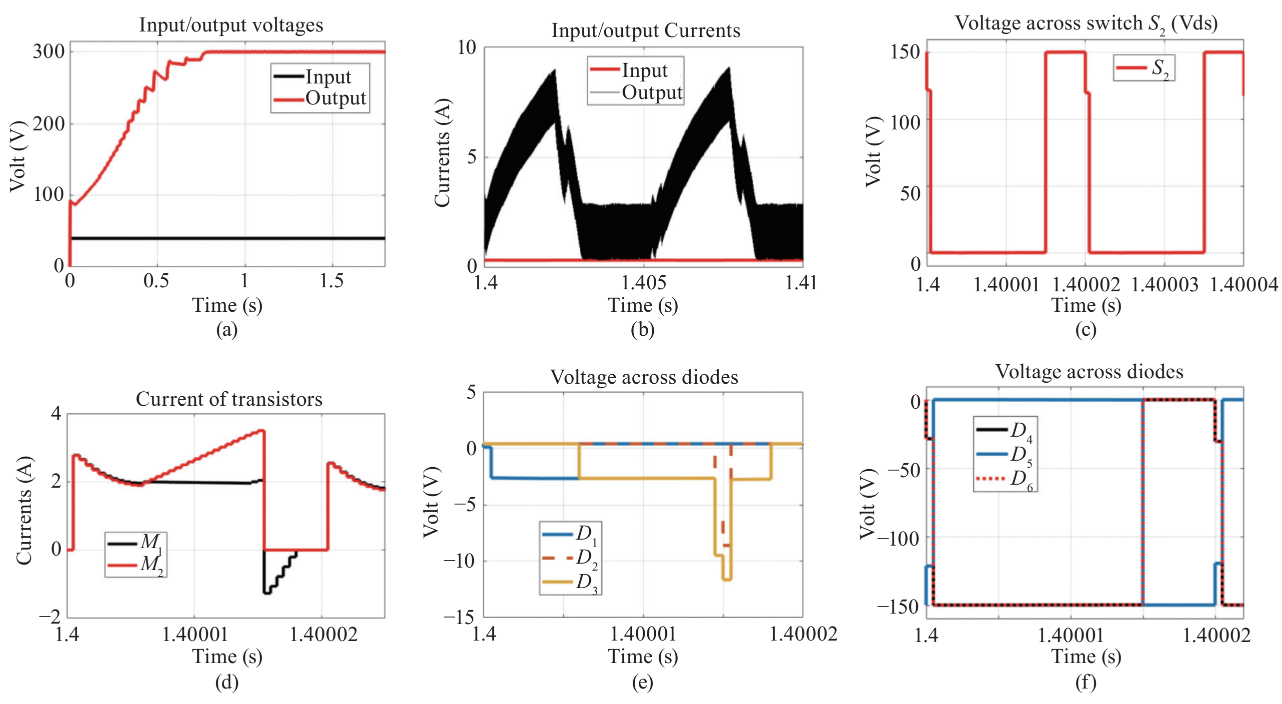

Fig. 9. (a) Input/output voltages, (b) input/output currents, (c) voltage and (d) current stresses of the switches. Voltage stresses for the (e) diodes D_1 to D_3 and (f) D_4 to D_6.

of input voltage source.

Figure 11(a) depicts experimental test workbench, whereas Figs. 18(b)–18(n) represent measured voltages and currents for the proposed converter. Switching frequency is 20 kHz, and inductors L_1, L_2, L_3, L_4 have an inductance of 200 μH. Capacitors C_1, and C_2 are set to 100 μF, C_3, C_4 are set to 47 μF, and Co is set to 470 μF. As to the load, a resistive load of 1.5 kΩ is used.

Figure 12(b) shows employing a 36 VDC voltage source produces a voltage close to 300 VDC. In addition, differential probes are used to monitor voltages and currents, with volume on the probe set to ×20. This means multiplying value displayed on the oscilloscope by 20.

As expected, a voltage equal to 85VDC is achieved for the switch S_2's drain-source pins. This can be seen in Fig. 18(c). This figure also shows switching voltage for gate-source pins of this switch. Fig. 11(d) shows voltages across inductors L_1 and L_2. The intriguing outcome is all of these inductors are being charged and discharged at the same time. Figs. 11(e) and 11(f) show voltage on capacitors C_1 to C_4. Greatest voltage is provided for capacitors closest to output nodes, as predicted. Maximum voltage for C_3 and C_4 is reported. Voltage and current stresses on components are one of the most significant characteristics of a successful converter. Voltage strains on diodes D_1 through D_6 are depicted in Figs. 11(g), 11(h), and 11(i). Because voltage at input side of converter is less than voltage at output nodes, elements on input side should experience lower voltage shocks. As a result, voltage stress for diodes D_3 to D_6 is greater than voltage stress for diodes D_1–D_2.

Figures 11(j)–11(m) show current for various elements of the converter. As previously stated, because output voltage of a boost converter is substantially greater than input voltage, voltage stresses are greater for the elements closest to the

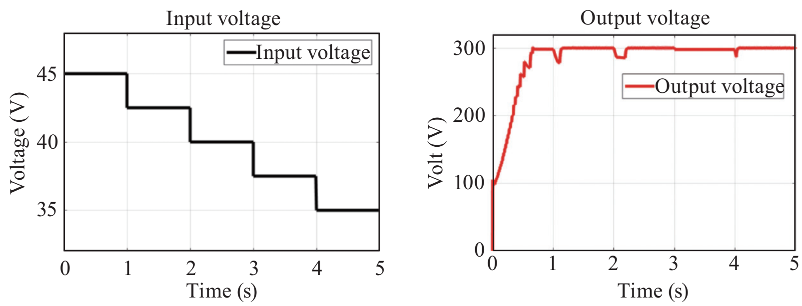

(a) (b)

Fig. 10. (a) Variable input voltage and (b) performance of the controller to fix the output voltage.

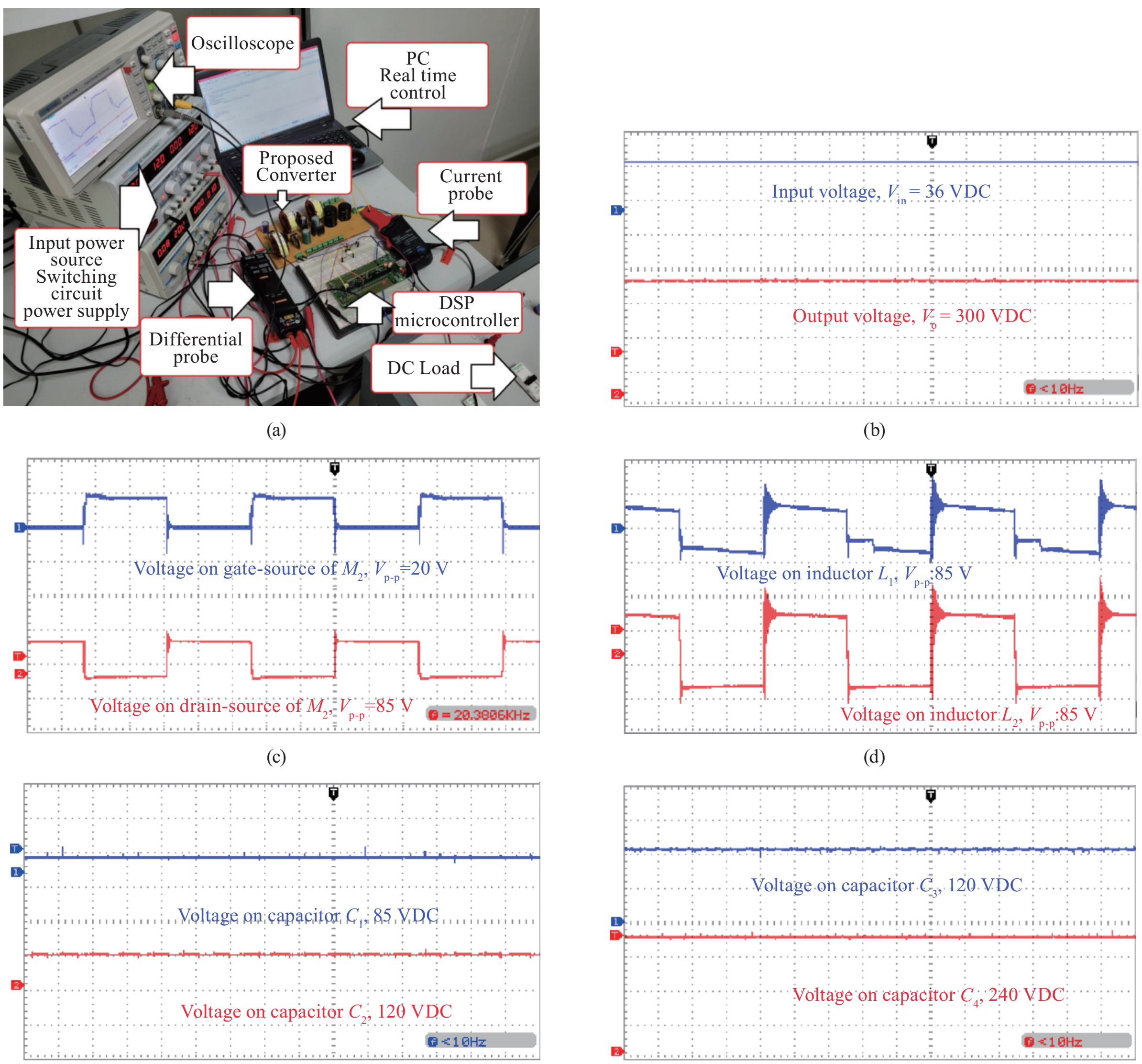

(a) (b)

(c) (d)

(e) (f)

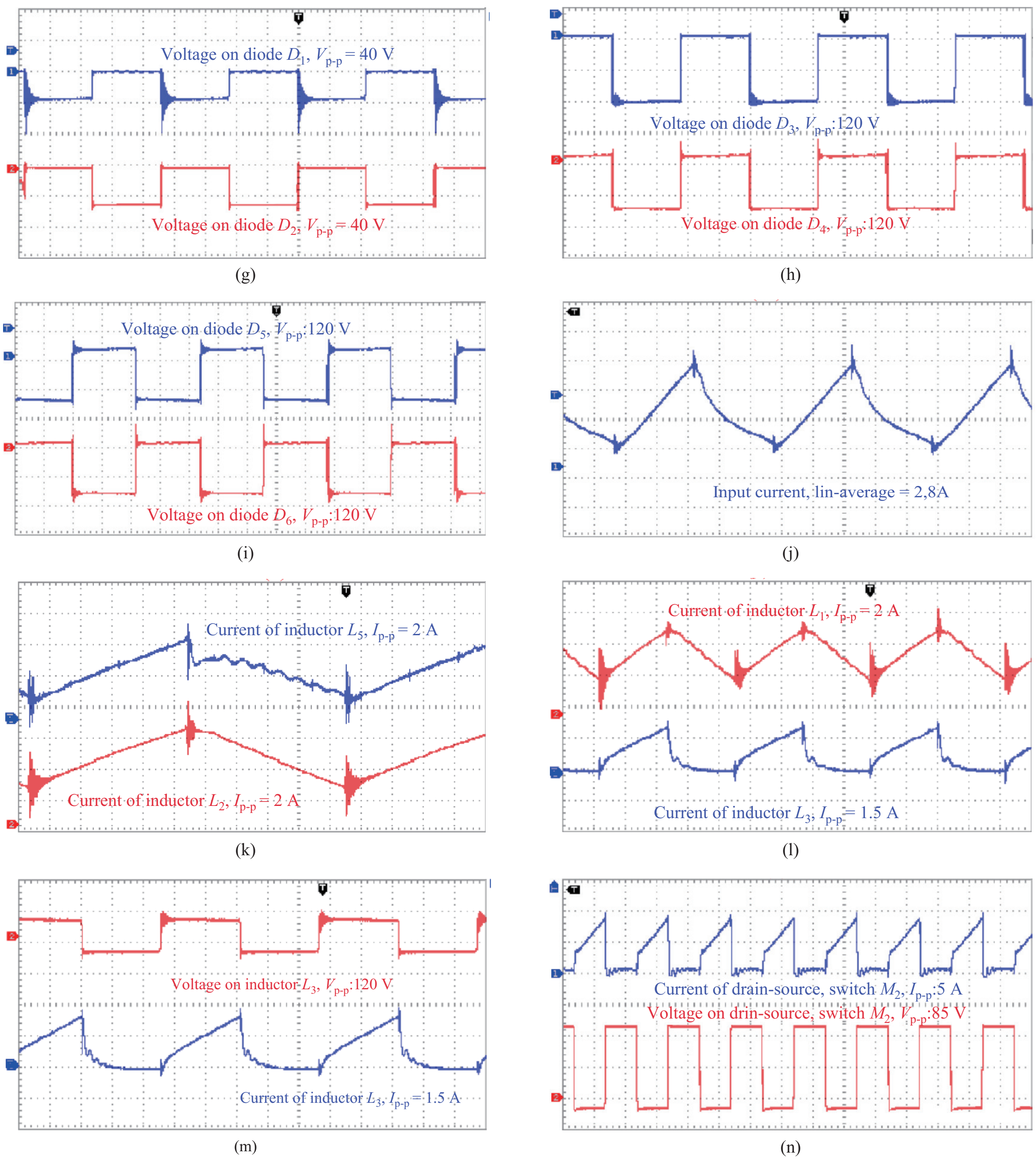

Fig. 11. (a) The hardware workbench, (b) input-output voltages, (c) gate-source and drain-source switching signals, voltage across the inductors (c) L_1, and L_2, (d) L_2, and L_3, (e) capacitors C_1, and C_2, (f) C_3, and C_4, voltage acroos the diodes (g) D_1, and D_2, (h) D_3, and D_4, (i) D_5, and D_6, (j) input current, current of (k) inductor L_1, (l) inductor L_2, (m) switch S_2, and (n) diode D_1.

output nodes. Instead, because input voltage is lower, current for elements on input side is higher for the same amount of power. Presented waveform has a power rating of around 100 W. As a result, as shown in Fig. 11(j), a current with an average of approximately 2.8 A is drawn from source.

Figures 11(k), 11(l), and 11(m) show current stresses for inductors L_1 to L_3. Fig. 11(n) shows current for switch S_2 as an example. Drain-source voltage of switch also is presented.

As previously stated, because output voltage of a boost converter is substantially greater than input voltage, voltage stresses are greater for elements closest to output nodes. Instead, because input voltage is lower, current for the elements on input side is higher for the same amount of power. The presented prototype converter has a power rating of around 220 W.

Figures 12(a) and 12(b) show test results for loss calculations at 220 W power. According to these figures, switching losses account for the majority of losses. A precise soft switching snubber circuit can reduce or eliminate this loss, resulting in improved efficiency. As a second overview, diodes are the primary source of power losses. In the second and third rows are switches and inductors. Efficiency diagram for suggested boost converter in modeling and experimental tests is shown in Fig. 13. Due to laboratory constraints, suggested

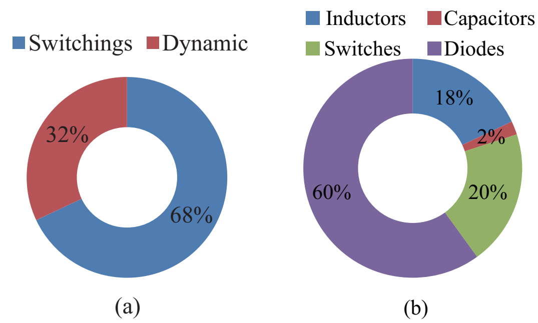

Fig. 12. (a) Distribution of switching and dynamic losses for the converter at 200 W. (b) Power losses distribution including dynamic and switching losses for all components.

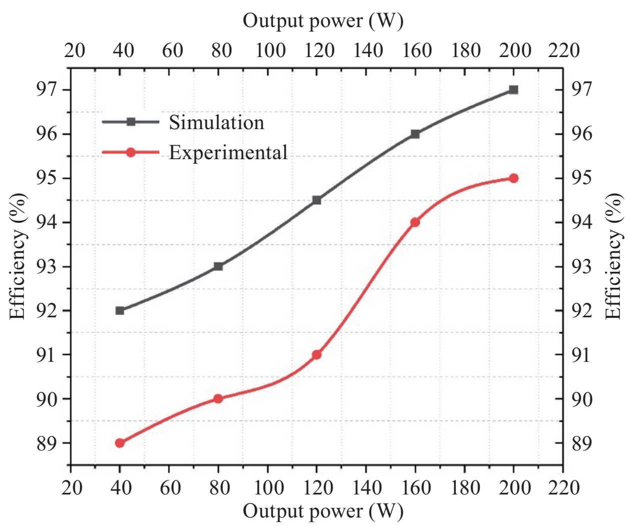

Fig. 13. Efficiency diagram of the proposed converter for simulation and experimental tests.

converter was tested at 220 W, but prototype converter was designed for 1.2 kW. Results reveal for the specified range of output powers, the suggested converter can exhibit higher efficiency for larger powers. Discrepancies between simulation and experimental testing can be expressed by taking into account real-time application conditions and component non-ideality.

IV. Conclusion

DC voltage generated by PV arrays is usually not in grid range, especially when only a little amount of energy is generated by a few panels. As a result, power converters in modern power transmission techniques should boost this voltage. MPPT converter, on the other hand, cannot generally fix generated voltage and is used to force panel to generate power at the maximum power point. This study presents a switched-inductor, switched-capacitor-based DC-DC power boost converter. By using duty ratios of 0.5 and 0.8, the suggested converter can boost input voltage by 6 and 18 times. Larger voltage gain is produced by cascading more switched capacitor cells, which easily double voltage created by converter and produce fewer current varieties as compared to switch inductor cells that are charged in parallel and discharged in series. The suggested converter includes only two power switches that switch simultaneously, reducing complexity of drive circuit's control mechanism. Simulation and experimental results are provided, including a simulation efficiency of more than 98 percent and an experimental efficiency of close to 96 percent. For larger power values, better efficiency can be obtained. The suggested converter is suitable for use in portable lighting systems, as well as PV-based off-grid or micro-grid applications. The recommended converter can be used for high-power applications by selecting appropriate high-power semiconductor devices and high-current inductors.

References

[1] A. A. Eladl, M. I. El-Afifi, M. A. Saeed, and M. M. El-Saadawi, "Optimal operation of energy hubs integrated with renewable energy sources and storage devices considering CO_2 emissions," *International Journal of Electrical Power & Energy Systems*, vol. 117, pp. 105719, May 2020.

[2] Y. S. Kim, "A voltage deviation-memorizing reactive power controller for renewable energy sources," *International Journal of Electrical Power & Energy Systems*, vol. 107, pp. 47–57, May 2019.

[3] Q. Qi, D. Ghaderi, and J. M. Guerrero, "Sliding mode controller-based switched-capacitor-based high DC gain and low voltage stress DC-DC boost converter for photovoltaic applications," *International Journal of Electrical Power & Energy Systems*, vol. 125, pp. 106496, Feb. 2021.

[4] M. Karaca, A. Mamizadeh, N. Genc, and A. Sular, "Analysis of passive filters for PV inverters under variable irradiances," in *2019 8th International Conference on Renewable Energy Research and Applications (ICRERA)*, 2019, pp. 680–685, doi: 10.1109/ICRERA47325.2019.8997111.

[5] R. X. Huang, F. Hong, and D. Ghaderi, "Sliding mode controller-based e-bike charging station for photovoltaic applications," *International Transactions on Electrical Energy Systems*, vol. 30, no. 4, pp. e12300, Apr. 2020.

[6] M. A. Celik, N. Genc, and H. Uzmus, "Experimental verification of interleaved hybrid DC/DC boost converter," *Journal of Power Electronics*, vol. 22, no. 10, pp. 1665–1675, Jun. 2022.

[7] D. Ghaderi, P. K. Maroti, P. Sanjeevikumar, J. B. Holm-Nielsen, E. Hossain, and A. Nayyar, "A modified step-up converter with small signal analysis-based controller for renewable resource applications," *Applied Sciences*, vol. 10, no. 1, pp. 102, Jan. 2020, doi: 10.3390/app10010102.

[8] G. Bayrak and D. Ghaderi, "An improved step-up converter with a developed real-time fuzzy-based MPPT controller for PV-based residential applications," *International Transactions on Electrical Energy Systems*, vol. 29, no. 12, pp. e12140, Dec. 2019, doi: 10.1002/2050-7038.12140.

[9] D. Ghaderi and G. Bayrak, "Performance assessment of a high-powered boost converter for photovoltaic residential implementations," *Elektronika Ir Elektrotechnika*, vol. 25, no. 6, pp. 40–47, Dec. 2019, doi: 10.5755/j01.eie.25.6.24825.

[10] D. Ghaderi and G. Bayrak, "A novel step-up power converter configuration for solar energy application," *Elektronika Ir Elektrotechnika*, vol. 25, no. 3, pp. 50–55, Jun. 2019, doi: 10.5755/j01.eie.25.3.23676.

[11] A. Ali, K. Almutairi, S. Padmanaban, V. Tirth, S. Algarni, K. Irshad, S. Islam, M. H. Zahir, M. Shafiullah, and M. Z. Malik, "Investigation of MPPT techniques under uniform and non-uniform solar irradiation condition–a retrospection," *IEEE Access*, vol. 8, pp. 127368–127392, Jul. 2020, doi: 10.1109/ACCESS.2020.3007710.

[12] S. R. Pendem and S. Mikkili, "Assessment of cross-coupling effects in PV string-integrated-converters with P&O MPPT algorithm under various partial shading patterns," *CSEE Journal of Power and Energy Systems*, vol. 8, no. 4, pp. 1013–1028, Jul. 2022, doi: 10.17775/CSEEJPES.2019.03330.

[13] A. Sangwongwanich and F. Blaabjerg, "Mitigation of interharmonics in PV systems with maximum power point tracking modification," *IEEE Transactions on power Electronics*, vol. 34, no. 9, pp. 8279–8282, Sep. 2019, doi: 10.1109/TPEL.2019.2902880.

[14] K. Kayisli, "Super twisting sliding mode-type 2 fuzzy MPPT control of solar PV system with parameter optimization under variable irradiance conditions," *Ain Shams Engineering Journal*, vol. 14, no. 1, pp. 101950, Feb. 2023, doi: 10.1016/j.asej.2022.101950.

[15] L. J. Gong, G. L. Hou, and C. Z. Huang, "A two-stage MPPT controller for PV system based on the improved artificial bee colony and simultaneous heat transfer search algorithm," *ISA Transactions*, vol. 132, pp. 428–443, Jan. 2023, doi: 10.1016/j.isatra.2022.06.005.

[16] P. K. Bonthagorla and S. Mikkili, "Performance investigation of hybrid and conventional PV array configurations for grid-connected/standalone PV systems," *CSEE Journal of Power and Energy Systems*, vol. 8, no. 3, pp. 682–695, May 2022, doi: 10.17775/CSEEJPES.2020.02510.

[17] B. P. Singh, S. K. Goyal, S. A. Siddiqui, A. Saraswat, and R. Ucheniya, "Intersection point determination method: a novel MPPT approach for sudden and fast changing environmental conditions," *Renewable Energy*, vol. 200, pp. 614–632, Nov. 2022, doi: 10.1016/j.renene.2022.09.056.

[18] S. R. Pendem and S. Mikkili, "Assessment of cross-coupling effects in PV string-integrated-converters with P&O MPPT algorithm under various partial shading patterns," *CSEE Journal of Power and Energy Systems*, vol. 8, no. 4, pp. 1013–1028, Jul. 2022, doi: 10.17775/CSEEJ PES.2019.03330.

[19] P. E. Kakosimos and A. G. Kladas, "Implementation of photovoltaic array MPPT through fixed step predictive control technique," *Renewable Energy*, vol. 36, no. 9, pp. 2508–2514, Sep. 2011, doi: 10.1016/j.rene ne.2011.02.021.

[20] A. Raj and R. P. Praveen, "Highly efficient DC-DC boost converter implemented with improved MPPT algorithm for utility level photovoltaic applications," *Ain Shams Engineering Journal*, vol. 13, no. 3, pp. 101617, May 2022, doi: 10.1016/j.asej.2021.10.012.

[21] C. S. Kumar and G. Mallesham, "A new hybrid boost converter with P & O MPPT for high gain enhancement of solar PV system," *Materials Today: Proceedings*, vol. 57, pp. 2262–2269, Jan. 2022, doi: 10.1016/j. matpr.2021.12.487.

[22] P. K. Pardhi, S. K. Sharma, and A. Chandra, "Grid-integrated single phase solar PV system employed with single switch high gain boost converter," *Electric Power Systems Research*, vol. 213, pp. 108231, Dec. 2022, doi: 10.1016/j.epsr.2022.108231.

[23] P. Upadhyay and R. Kumar, "A high gain cascaded boost converter with reduced voltage stress for PV application," *Solar Energy*, vol. 183, pp. 829–841, May 2019, doi: 10.1016/j.solener.2019.03.075.

[24] S. Saravanan and N. R. Babu, "Analysis and implementation of high step-up DC-DC converter for PV based grid application," *Applied Energy*, vol. 190, pp. 64–72, Mar. 2017, doi: 10.1016/j.apenergy.201 6.12.094.

[25] D. Venkatramanan and V. John, "Dynamic modeling and analysis of buck converter based solar PV charge controller for improved MPPT performance," *IEEE Transactions on Industry Applications*, vol. 55, no. 6, pp. 6234–6246, Nov./Dec. 2019.

[26] D. S. Pillai and N. Rajasekar, "An MPPT-based sensorless line–line and line–ground fault detection technique for PV systems," *IEEE Transactions on Power Electronics*, vol. 34, no. 9, pp. 8646–8659, Sep. 2019.

[27] M. Rezkallah, A. Chandra, M. Tremblay, and H. Ibrahim, "Experimental implementation of an APC with enhanced MPPT for standalone solar photovoltaic based water pumping station," *IEEE Transactions on Sustainable Energy*, vol. 10, no. 1, pp. 181–191, Jan. 2019.

[28] J. Baek, J. K. Kim, J. B. Lee, M. H. Park, and G. W. Moon, "A new standby structure integrated with boost PFC converter for server power supply," *IEEE Transactions on Power Electronics*, vol. 34, no. 6, pp. 5283–5293, Jun. 2019.

[29] M. Veerachary and P. Shaw, "Analysis and design of CD-cell-based fifth-order boost converter with robust stability considerations," *IEEE Transactions on Industry Applications*, vol. 55, no. 6, pp. 7491–7504, Nov./Dec. 2019.

[30] A. Bag, B. Subudhi and P. K. Ray, "A combined reinforcement learning and sliding mode control scheme for grid integration of a PV system," *CSEE Journal of Power and Energy Systems*, vol. 5, no. 4, pp. 498–506, Dec. 2019, doi: 10.17775/CSEEJPES.2017.01000.

[31] S. W. Lee and H. L. Do, "High step-up coupled-inductor cascade boost DC-DC converter with lossless passive snubber," *IEEE Transactions on Industrial Electronics*, vol. 65, no. 10, pp. 7753–7761, Oct. 2018.

[32] S. H. Chincholkar, W. T. Jiang, and C. Y. Chan, "An improved PWM-based sliding-mode controller for a DC-DC cascade boost converter," *IEEE Transactions on Circuits and Systems II: Express Briefs*, vol. 65, no. 11, pp. 1639–1643, Nov. 2018.

[33] Y. M. Ye and K. W. E. Cheng, "Quadratic boost converter with low buffer capacitor stress," *IET Power Electronics*, vol. 7, no. 5, pp. 1162–1170, May 2014.

[34] T. Roy and P. K. Sadhu, "A step-up multilevel inverter topology using novel switched capacitor converters with reduced components," *IEEE Transactions on Industrial Electronics*, vol. 68, no. 1, pp. 236–247, Jan. 2021.

[35] T. Shamsi, M. Delshad, E. Adib, and M. R. Yazdani, "A new simple-structure passive lossless snubber for DC–DC boost converters," *IEEE Transactions on Industrial Electronics*, vol. 68, no. 3, pp. 2207–2214, Mar. 2021.

[36] K. Mozaffari and M. Amirabadi, "A reduced-switch-count family of soft-switched high-frequency inductive AC-link converters," *IEEE Transactions on Power Electronics*, vol. 35, no. 8, pp. 7972–7990, Aug. 2020.

[37] K. Yao, X. Ruan, C. Zou, and Z. Ye, "Three-phase single-switch boost power factor correction converter with high input power factor," *IET Power Electronics*, vol. 5, no. 7, pp. 1095–1103, Aug. 2012.

[38] K. I. Hwu and T. J. Peng, "High-voltage-boosting converter with charge pump capacitor and coupling inductor combined with buck-boost converter," *IET Power Electronics*, vol. 7, no. 1, pp. 177–188, Jan. 2014.

[39] G. H. Zhou, G. H. Mao, H. B. Zhao, S. H. Zhou, and P. Mattavelli, "Digital average-ripple-based control techniques for switching converters with fast transient performance," *IEEE Journal of Emerging and Selected Topics in Power Electronics*, vol. 9, no. 1, pp. 89–101, Feb. 2021.

[40] L. L. Zhao, Y. F. Wu, Z. Y. Chen, L. X. Shen, and C. H. Zhang, "The current sharing strategy of three-phase series capacitor boost converter based on charge-balance method," *IEEE Transactions on Power Electronics*, vol. 36, no. 4, pp. 4864–4876, Apr. 2021.

[41] H. S. Xu, D. Y. Chen, F. Xue, and X. T. Li, "Optimal design method of interleaved boost PFC for improving efficiency from switching frequency, boost inductor, and output voltage," *IEEE Transactions on Power Electronics*, vol. 34, no. 7, pp. 6088–6107, Jul. 2019.

[42] J. W. Zhao, D. L. Chen, and J. H. Jiang, "A novel transformerless high step-up DC-DC converter with active switched-inductor and quasi-Z-source network," *IET Power Electronics*, vol. 14, no. 9, pp. 1592–1605, Jul. 2021, doi: 10.1049/pel2.12128.

[43] H. Z. Li, L. H. Cheng, X. J. Sun, and C. Li, "High step-up combined boost-Cuk converter with switched-inductor," *IET Power Electronics*, vol. 15, no. 15, pp. 1664–1674, Nov. 2022, doi: 10.1049/pel2.12335.

[44] T. Yao, C. H. Nan, and R. Ayyanar, "A new soft-switching topology for switched inductor high gain boost," *IEEE Transactions on Industry Applications*, vol. 54, no. 3, pp. 2449–2458, May/Jun. 2018.

[45] K. B. Park, G. W. Moon, and M. J. Youn, "Nonisolated high step-up boost converter integrated with sepic converter," *IEEE Transactions on Power Electronics,* vol. 25, no. 9, pp. 2266–2275, Sep. 2010.

[46] E. Babaei, T. Jalilzadeh, M. Sabahi, M. Maalandish, and R. S. Alishah, "High step-up DC-DC converter with reduced voltage stress on devices," *International Transactions on Electrical Energy Systems*, vol. 29, no. 4, pp. e2789, Apr. 2018.

[47] S. Pirpoor, S. Rahimpour, M. Andi, N. Kanagaraj, S. Pirouzi, and A. H. Mohammed, "A novel and high-gain switched-capacitor and switched-inductor-based DC/DC boost converter with low input current ripple and mitigated voltage stresses," *IEEE Access*, vol. 10, pp. 32782–32802, Mar. 2022, doi: 10.1109/ACCESS.2022.3161576.

[48] O. Abdel-Rahim and H. Y. Wang, "A new high gain DC-DC converter with model-predictive-control based MPPT technique for photovoltaic systems," *CPSS Transactions on Power Electronics and Applications*, vol. 5, no. 2, pp. 191–200, Jun. 2020, doi: 10.24295/CPSSTPEA.2020 .00016.

[49] C. P. Rao, A. Hajjiah, M. A. El-Meligy, M. Sharaf, A. T. Soliman, and M. A. Mohamed, "A novel high-gain soft-switching DC-DC converter with improved P&O MPPT for photovoltaic applications," *IEEE Access*, vol. 9, pp. 58790–58806, Apr. 2021.

[50] H. Tekin, K. Bulut, and D. Ertekin, "A novel switched-capacitor and fuzzy logic-based quadratic boost converter with mitigated voltage stress, applicable for DC micro-grid," *Electrical Engineering*, vol. 104, no. 6, pp. 4391–4413, Aug. 2022, doi: 10.1007/s00202-022-01631-3.

Davut Ertekin received the Ph.D. degree in Electrical Engineering from Ataturk University, Erzurum, Turkey, in 2017. In 2019, he went to Politecnico di Bari, Italy, as a Lecturer for short-term education in the Department of Electrical and Information Engineering. He has also worked as the Chief of power drive circuits of radiographic generators and systems production company in Ankara, Turkey, from September 2014 to February 2018. He is currently an Assistant Professor with the Department of Electrical and Electronics Engineering, Bursa Technical University, Bursa, Turkey. His area of focus is power transmission techniques and power electronics. His current research interests include reliability studies and material analysis for DC–DC power converters components applicable for renewable energy power transmission, inverters, and controller designs for these converters. He is currently the Reviewer of the IEEE Transactions on Power Electronics, the IEEE Transactions on Industrial Electronics, IEEE Access, International Transactions on Electrical Energy Systems (Wiley), and many other SCI journals. He has published 25 SCI-indexed papers in field of power electronics and the power converters in grid connected renewable energy systems.